



Optical complex media as universal reconfigurable linear operators

MAXIME W. MATTHÈS,¹ PHILIPP DEL HOUGNE,¹  JULIEN DE ROSNY,¹ GEOFFROY LEROSEY,² AND SÉBASTIEN M. POPOFF^{1,*} 

¹Institut Langevin, CNRS UMR 7587, ESPCI Paris, PSL Research University, 1 rue Jussieu, 75005 Paris, France

²Greenerwave, ESPCI Paris Incubator PC'up, 6 rue Jean Calvin, 75005 Paris, France

*Corresponding author: sebastien.popoff@espci.psl.eu

Received 14 January 2019; revised 5 March 2019; accepted 19 March 2019 (Doc. ID 357157); published 10 April 2019

Performing linear operations using optical devices is a crucial building block in many fields ranging from telecommunications to optical analog computation and machine learning. For many of these applications, key requirements are robustness to fabrication inaccuracies, reconfigurability, and scalability. We propose a way to perform linear operations using complex optical media such as multimode fibers or scattering media as a computational platform driven by wavefront shaping. Given a large random transmission matrix representing light propagation in such a medium, we can extract any desired smaller linear operator by finding suitable input and output projectors. We demonstrate this concept by finding input wavefronts using a spatial light modulator that cause the complex medium to act as a desired complex-valued linear operator on the optical field. We experimentally build several 16×16 operators and discuss the fundamental limits of the scalability of our approach. It offers the prospect of reconfigurable, robust, and easy-to-fabricate linear optical analog computation units. © 2019 Optical Society of America under the terms of the OSA Open Access Publishing Agreement

<https://doi.org/10.1364/OPTICA.6.000465>

1. INTRODUCTION

The ability to perform linear operations on light with optical devices is a fundamental ingredient in many areas of optics and photonics, including signal processing and spatial multiplexing in optical communication, as well as optical analog computation. For emerging applications to optical artificial neural networks, the ability to reconfigure these linear photonic processing units is crucial. Moreover, ease of fabrication and robustness to manufacturing inaccuracies are highly sought-after features. Similar to electronic devices, photonic devices are traditionally designed to perform one given operation [1–5]. The conformation of the device is directly linked to its intended function. As a consequence, fabrication imperfections and changes of environmental conditions negatively affect its functioning, limiting the range of operation of the device. Furthermore, such inverse-design approaches inherently prohibit reconfigurability.

Programmable coherent photonic circuits have the potential to offer reconfigurability. Initially conceived in free-space optics by leveraging beamsplitters [6], recent advances in silicon photonics also enabled the implementation of the concept in integrated designs [7–12]. Several first experimental demonstrations of this approach have produced promising results. However, the amount of phase shifters required in these architectures scales with the square of the size of the desired transformation, which raises questions about the overall scalability of the approach. Alternatively, the idea of controlling mode coupling inside a multimode

waveguide to shape the output wavefront was demonstrated using silicon-on-insulator planar waveguides whose index profile can be tuned using femtosecond laser pulses [13]. Another approach using multiplane modulation was proposed [14] and was successfully used for few mode manipulations [15]. While small transformations may suffice for optical communications, the increasing complexity of the physical system may hinder the implementation of the high rank transformations needed in optical analog computation. There is currently no solution to perform optical linear operations involving a high number of channels.

Parallel to the aforementioned developments, since Vellekoop and Mosk's landmark paper in 2007 [16] the field of wavefront shaping in complex media emerged [17,18]. A complex medium may be defined as a system that mixes the spatial and/or temporal degrees of freedom, resulting in the complete scrambling of an incident wavefront [19]. Examples include chaotic cavities, disordered waveguides, or random scattering systems such as paint layers or biological tissues [16,17,20–25]. The seemingly random effect of the disorder on the wavefront is deterministic; hence, such a system can be fully represented by a linear transmission matrix (TM) [20]. Due to the large number of modes, those matrices have large dimensions. Moreover, the lack of symmetry of the system contributes to the TM's high rank. By injecting light into a well-chosen combination of input modes using a spatial light modulator (SLM), an optical scattering medium can be used to perform a wide variety of functions. Initial efforts sought to

overcome the scrambling of the wavefront in space and/or time through wavefront shaping (e.g., to focus behind or transmit information through a complex medium) [16,20,25–30]. Strikingly, it was possible to beat the Rayleigh limit on focusing [31,32] and the Nyquist–Shannon sampling theorem [33].

Despite its potential, controlling wave propagation in complex media to perform linear transformations has received little attention. The literature contains reports on implementations of two-port beamsplitters [34,35], with applications to control quantum interferences in mind [36,37], as well as on spatial mode sorting [38]. In particular, the possibility to implement large reconfigurable linear transformations as required for optical neural networks has remained unexplored to date. Building on recent work that demonstrated wave-based analog computation in a chaotic microwave cavity [39], we explore here the possibility to perform large complex-valued linear operations in optical complex media. We formulate fundamental upper bounds in terms of the operation size that can be implemented in a realistic optical system. Moreover, we experimentally demonstrate the possibility to take advantage of the large number of degrees of freedom of a disordered optical system (multimode fiber or glass diffuser) of which we acquire the transmission matrix (TM), to physically perform different desired linear transformations. We aim to provide an implementation of reconfigurable optical linear transformations that meets the necessary criteria for real-life implementations (i.e., minimal hardware requirements, low stability requirements, and short reconfiguration times). To that end, we do not rely on interferometric phase measurements; instead, we leverage phase retrieval techniques, eliminating the need for high mechanical stability. We use fast binary modulators that allow above 10 kHz refresh rates. Moreover, the one-off calibration of the medium’s TM allows us to reconfigure the implemented linear transformation without any further experimental measurement.

2. OPERATION PRINCIPLE

A. Principle

Light propagation through a linear disordered system at a given frequency is fully described by its transmission operator \mathbf{H} that links the output state of light $|\psi_{\text{out}}\rangle$ to the input one $|\psi_{\text{in}}\rangle$, so

$$|\psi_{\text{out}}\rangle = \mathbf{H}|\psi_{\text{in}}\rangle. \quad (1)$$

Usually, only a small subset of the input and output modes are controlled and measured. Then, the transmission matrix has the statistical properties of an ideal random Gaussian matrix [40,41]. If one controls N input modes and measures M output modes, \mathbf{H} is represented by a $M \times N$ matrix and $|\psi_{\text{in}}\rangle$ (resp $|\psi_{\text{out}}\rangle$) is represented by a vector of size N (resp. M). Suppose we seek to create a system performing a linear operation represented by the matrix \mathbf{G} of size $m \times n$ with $m < M$ and $n < N$. Once the complex medium’s transmission matrix \mathbf{H} is measured, we want to identify adequate input and output projections to perform the desired linear operation with the system. These projections are represented by $N \times n$ and $M \times m$ input and output matrices, \mathbf{P}_{in} and \mathbf{P}_{out} , that satisfy

$$\mathbf{G} = \mathbf{P}_{\text{out}}^T \mathbf{H} \mathbf{P}_{\text{in}}. \quad (2)$$

B. Input and Output Projectors

We limit ourselves to input projectors \mathbf{P}_{in} that can be created by modulating the optical field at a given input plane (i.e., using a

SLM). We divide the SLM into n groups of N/n pixels on which we control the amplitude and/or the phase of the optical field. The output projection \mathbf{P}_{out} is realized by measuring m speckle grains at the output plane.

For illustration purposes, we use $n = m = 4$. The corresponding projectors \mathbf{P}_{in} and \mathbf{P}_{out} have the following matrix representations,

$$\mathbf{P}_{\text{in}} = \begin{bmatrix} p_{1,1} & 0 & 0 & 0 \\ \vdots & \vdots & \vdots & \vdots \\ p_{N/4,1} & 0 & 0 & 0 \\ 0 & p_{1,2} & 0 & 0 \\ \vdots & \vdots & \vdots & \vdots \\ 0 & p_{N/4,2} & 0 & 0 \\ 0 & 0 & p_{1,3} & 0 \\ \vdots & \vdots & \vdots & \vdots \\ 0 & 0 & p_{N/4,3} & 0 \\ 0 & 0 & 0 & p_{1,4} \\ \vdots & \vdots & \vdots & \vdots \\ 0 & 0 & 0 & p_{N/4,4} \end{bmatrix}, \quad \mathbf{P}_{\text{out}} = \begin{bmatrix} 1 & 0 & 0 & 0 \\ 0 & 1 & 0 & 0 \\ 0 & 0 & 1 & 0 \\ 0 & 0 & 0 & 1 \\ 0 & 0 & 0 & 0 \\ \vdots & \vdots & \vdots & \vdots \\ 0 & 0 & 0 & 0 \end{bmatrix}, \quad (3)$$

where $p_{k,l}$, $(k, l) \in [1, N/4] \otimes [1, 4]$ represents the modulation on the l th pixel of the k th segments of the modulator. For the sake of simplicity, the output projection is done here by taking the first four elements of the output basis.

C. Existence of Solution with Ideal Modulation and Theoretical Limits

We assume the ideal case of \mathbf{H} being a Gaussian random matrix measured with negligible noise and the spatial modulation scheme being able to control with high fidelity the amplitude and the phase of the field. The Gaussian matrix approximation is known to be valid when one controls and measures a fraction of the total number of modes [40]. Satisfying the equality of Eq. (2) with the projectors as represented by Eq. (3) consists in solving n systems of m linear equations, so

$$\mathbf{H}_{k\perp} \begin{bmatrix} p_{1,k} \\ p_{2,k} \\ \vdots \\ p_{N/n,k} \end{bmatrix} = \mathbf{G}_k \quad \text{for } k \in [1, n], \quad (4)$$

with $\mathbf{H}_{k\perp} = \mathbf{P}_{\text{out}}^T \mathbf{H}_k$ the m by N/n subpart of \mathbf{H} corresponding to the transmission matrix that links the pixels of the k th part of

the SLM to the m selected outputs on the camera. \mathbf{G}_k is the k th column of the target matrix \mathbf{G} . If a solution exists, it can be written as

$$\begin{bmatrix} p_{1,k} \\ p_{2,k} \\ \vdots \\ p_{N/n,k} \end{bmatrix} = \mathbf{H}_{k\perp}^+ \mathbf{G}_k, \quad (5)$$

with $\mathbf{H}_{k\perp}^+$ the Moore–Penrose inverse (pseudo-inverse) of $\mathbf{H}_{k\perp}$. Such a solution exists if $\mathbf{H}_{k\perp}$ has linearly independent rows. Because $\mathbf{H}_{k\perp}$ is a Gaussian random matrix with independent identically distributed elements, it can be eigendecomposed and its singular value distribution follows the Marchenko–Pastur law [42]. For large matrices, the probability of having a zero singular value vanishes for $N/n > m$, ensuring that $\mathbf{H}_{k\perp}^+$ exists and that $\mathbf{H}_{k\perp}^+ \mathbf{G}_k$ is a solution. If one can independently control the amplitude and the phase of the optical field, the complex mask corresponding to Eq. (5) can be implemented. We thus find that for a full complex field modulation, it is sufficient to control $M = n \times m$ independent channels of the complex system to be able to correctly simulate the target matrix \mathbf{G} . While other types of media may allow Eq. (2) to be satisfied, the random nature of complex media ensures the existence of a trivial solution regardless of the complexity of the target operator \mathbf{G} .

Note that no hypothesis has been made on the operator \mathbf{G} . It demonstrates the universality of the approach to perform any linear transformation. Experimentally, the passive modulation of the SLM imposes $|p_{i,j}| < 1 \forall (i, j) \in [1, N/n] \times [1, n]$. It limits the applications to operators with below unity singular values. However, for any operator \mathbf{G} , the experimental system we present can simulate the transformation corresponding to the operator $\mathbf{G}' = \alpha \mathbf{G}$ with $\alpha \leq 1$ chosen so that the largest singular value of \mathbf{G}' is smaller than 1.

3. EXPERIMENT

A. Optical Setup

To illustrate the versatility of our approach, we report two experimental implementations of our scheme using two very different complex media as optical processing units: a multimode fiber and a ground glass diffuser at two different wavelengths (respectively, 1550 nm and 632.8 nm). For both experiments, we modulate the impinging wavefront with a digital micromirror device (DMD).

The MMF experiment uses a 1 m long segment of a step index fiber of numerical aperture (NA) 0.22 with a core diameter of 105 μm supporting approximately 2000 guided modes. The light source is a 1.55 μm telecom narrow-band laser (PS-NLL, TeraXion). We use a 1920 \times 1200 pixel, 16 kHz digital micromirror device (V-9601, ViALUX GmbH) for the modulation. The output intensity pattern is imaged onto a fast 640 \times 512 pixel InGaAs camera (Cheetah 640CL, Xenics). The fiber is compressed at four different locations to ensure strong mode coupling [43]. The scattering media setup uses a ground glass diffuser (DG20-1500, Thorlabs) with a 632.8 nm laser source (1137/P, JDSU Uniphase) modulated by a 2560 \times 1600 pixel, 12 kHz DMD (V-9001, ViALUX GmbH) and a 2336 \times 1752 pixel CCD camera (Prosilica GT2300, Allied Vision). The MMF setup is depicted in Fig. 1, and the scattering medium setup is schematically similar. The number of controlled segments on the DMD is

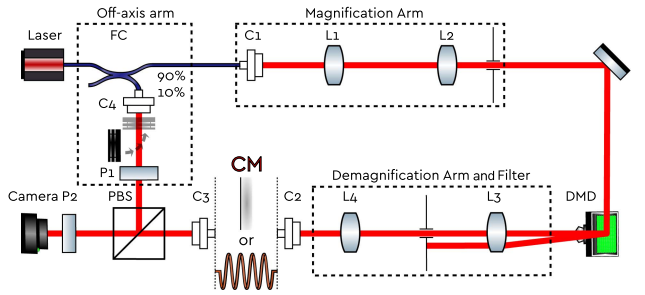


Fig. 1. Schematic representation of the setup. An expanded laser beam is modulated after reflection off a DMD and injected into a complex medium (CM: ground glass diffuser or multimode fiber). One polarization of the outgoing light is recorded by a digital camera. A reference arm is used only for the final estimation of the fidelity to measure the complex optical field for the MMF experiment. FC: fiber coupler; Ci (with $i \in [1 \dots 4]$): fiber collimator; Li (with $i \in [1 \dots 4]$): planoconvex lens; PBS: polarization beamsplitter; and P1 and P2: polarizers.

$N = 1568$ for the MMF experiment and $N = 2304$ for the scattering media. Both complex media stay highly correlated during the time of the experiment: The output intensity patterns show correlations greater than 98% for about 2 h. (Supplement 1 provides the details and correlation curves.)

B. Procedure

The steps of the procedure are schematically illustrated in Fig. 2. A first calibration step consists in learning the TM of the complex propagation medium, namely a multimode fiber or a scattering medium. The second step consists in numerically finding the optimal projectors \mathbf{P}_{in} and \mathbf{P}_{out} that best satisfy Eq. (2) for a given operator \mathbf{G} knowing the transmission matrix \mathbf{H} . Finally, by displaying the corresponding masks onto the SLM and measuring the field on the designated outputs, the system acts as the target operator \mathbf{G} on the incident field. Those three steps are discussed in detail in the following sections.

1. Calibration

We first estimate the medium's complex-valued transmission matrix \mathbf{H} . To remove the need for interferometric measurements, which requires high mechanical stability that limits the versatility of the approach, and to mitigate the effect of measurement errors, we use a phase retrieval algorithm. It allows the recovery of the full TM from intensity-only measurements [44,45]. We divide the pixel array of the DMD into N groups of pixels or *macropixels*. We then send a learning set of $7N$ random binary vectors (entries have zero or unity amplitude) and measure the corresponding output intensity patterns on the camera. These patterns are projected onto an output basis of macropixels of a size that corresponds to a speckle grain. The obtained data is fed into a phase retrieval algorithm [45] and the results are further refined using a gradient descent optimization to better account for the nonlinearity of the camera response (see Supplement 1).

We reconstruct matrices of size 100 \times 1568 for the MMF setup and 100 \times 2304 for the scattering medium. The computation is accelerated through parallelization with a graphical processing unit (GPU) (GeForce GTX 1050 Ti, NVIDIA) and is completed in under 2 min. We evaluate the quality of the reconstructed TM using test input wavefronts that have not been used

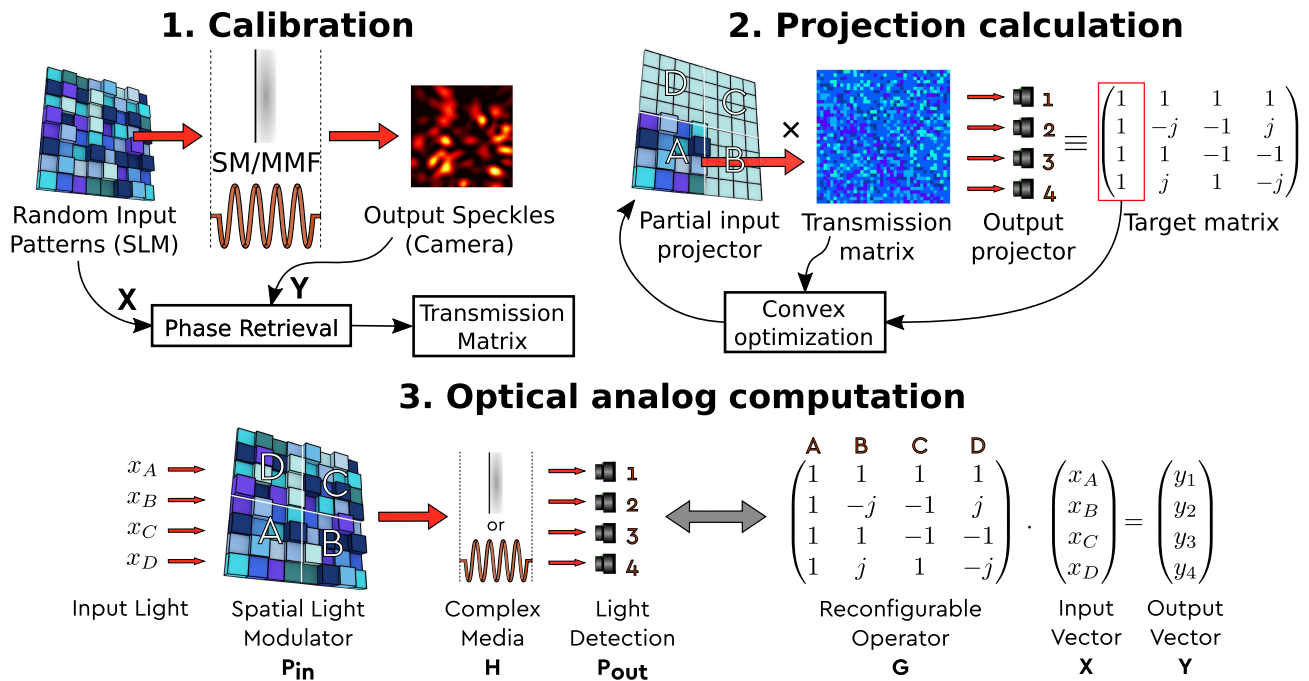


Fig. 2. Overview of the experimental procedure for performing a DFT operation of size 4 ($n = m = 4$ and $\mathbf{G} = \text{DFT}_4$). Step 1: System calibration. Acquisition of the complex TM by measuring a set of input patterns and output intensity speckles and using a phase retrieval algorithm. Step 2: Optimal input projection calculation. We illustrate the procedure by showing how to find one subpart of the input mask. The computation is done independently for each subpart of the SLM using a convex optimization solver and using the TM and the corresponding column of the target matrix \mathbf{G} as inputs. Step 3: Analog computation. The proposed optical processing unit is composed of a spatial light modulator (SLM) and a complex medium. The SLM and the output detection take the role of the projectors \mathbf{P}_{in} and \mathbf{P}_{out} , converting the given transmission matrix \mathbf{H} of the complex medium into a desired linear transformation \mathbf{G} [see Eq. (2)].

for the learning procedure by calculating the root mean square error (RMSE) for each element of the output basis, giving $\text{RMSE}_{\text{mean}} \sim 7\%$ ($\text{std}(\text{RMSE}_{\text{mean}}) \sim 6\%$ and $\text{RMSE}_{\text{median}} < 5\%$) for the MMF setup, and $\text{RMSE}_{\text{mean}} \sim 11.6\%$ ($\text{std}(\text{RMSE}_{\text{mean}}) \sim 7.3\%$ and $\text{RMSE}_{\text{median}} < 7.9\%$) for the visible setup.

2. Projection Calculation

The output projection \mathbf{P}_{out} is realized by selecting m output speckle grains. The optical fields in these areas correspond to the output of our operator. We choose the output points that give the lowest reconstruction error during the calibration step. We then obtain the output projection as represented in Eq. (3), where rows are ordered from the lowest to the highest error.

We demonstrated that for a full amplitude and phase modulation, the input masks corresponding to the optimal input projectors \mathbf{P}_{in} can readily be calculated from the TM using the relation 5. Using binary amplitude modulators, we achieve a few-level modulation of the optical phase using Lee holograms (see Supplement 1). The modulated beam is then projected onto the complex medium. We collect the output intensity pattern for a single polarization using a digital camera. Identifying an input mask on the DMD that approximates the equality in Eq. (2) for a given target matrix \mathbf{G} is an ill-posed problem since we do not have full control over the complex wavefront. Finding an input projector \mathbf{P}_{in} that minimizes $\|\mathbf{G} - \mathbf{P}_{\text{out}}^T \mathbf{H} \mathbf{P}_{\text{in}}\|_2$ with the constraint of looking for solutions with discrete phase values is a convex problem. We use a mixed-integer convex solver [46,47] to find an approximate solution that satisfies the experimental restrictions of the few-level wavefront modulation of the DMD

(see Supplement 1). The computation of the input projector \mathbf{P}_{in} takes less than 20 min for 16×16 operators and under 5 min for 8×8 operators on a computer with an Intel i7-7700 CPU with 32 GB or RAM running on Windows 10.

3. Optical Analog Computation

Once the appropriate input projector mask is calculated and displayed on the DMD, the system is ready to act like the desired linear operator \mathbf{G} . The operation is performed on a desired input vector by encoding its components $\mathbf{X} = (x_1, x_2, \dots, x_n)^T$ into as many light beams directed toward the SLM and collecting the output vector \mathbf{Y} on the detection device such that

$$\mathbf{Y} = \mathbf{G}\mathbf{X} = \mathbf{P}_{\text{out}}^T \mathbf{H} \mathbf{P}_{\text{in}} \mathbf{X}. \tag{6}$$

In principle, the input information is encoded into the optical field values impinging on the different segments of the DMD. To limit the complexity of the experimental setup, input vectors are directly encoded using the DMD. To do so, each subpart of the input projection is modulated by the value of the corresponding component of the incoming input vector \mathbf{X} . This allows us to work with a single incoming light beam, but limits the modulation to only a few levels (see Supplement 1).

4. RESULTS

We illustrate the reconfigurability of the presented scheme by experimentally implementing two linear transformations very common in computer and physical science; namely, the discrete Fourier transform and the Hadamard matrix. Their general expressions read

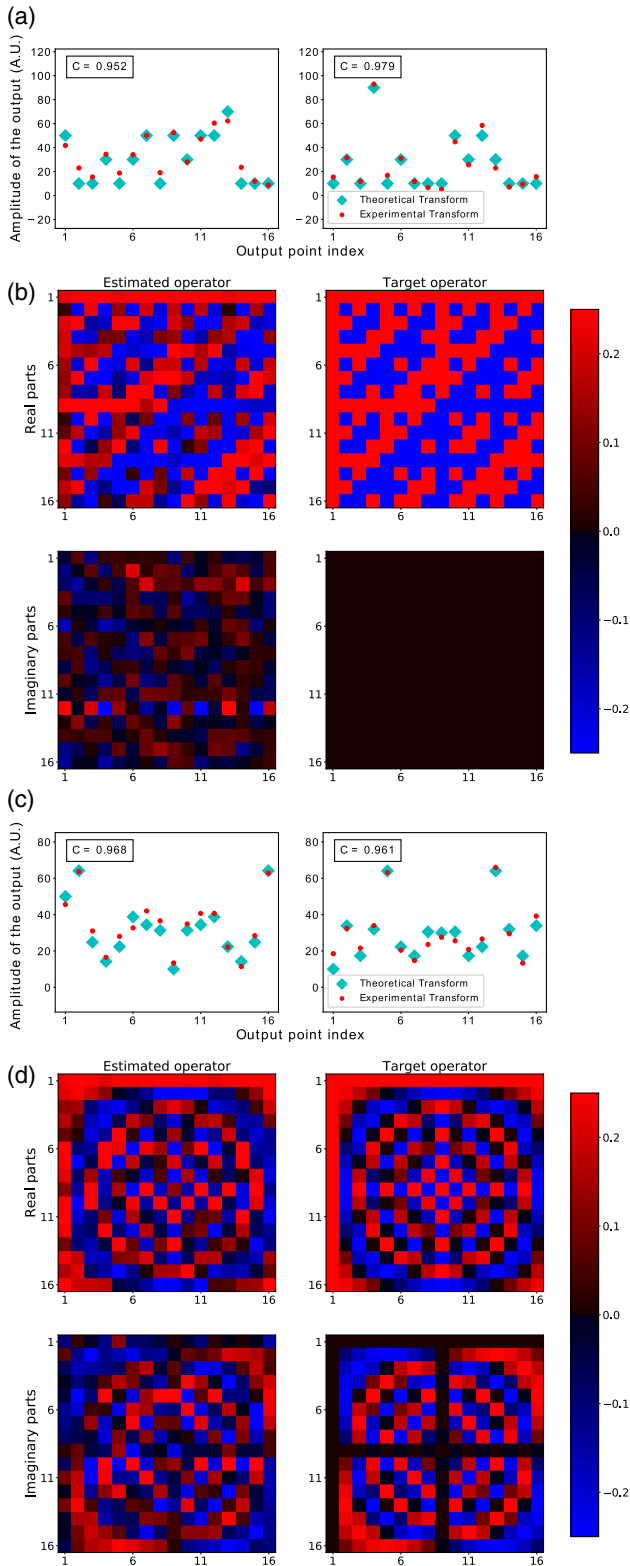


Fig. 3. Comparison of experimentally implemented operators and target operators. We use as target matrix \mathbf{G} , a 16×16 Hadamard matrix [(a) and (b)], and a 16×16 discrete Fourier transform [(c) and (d)]. Absolute values of experimental (red dots) and theoretical (cyan diamonds) results of the linear transformations for two different random input vectors drawn from $\{-1, 0, 1\}$ for $\mathbf{G} = \text{Ha}_{16}$ (a) and $\mathbf{G} = \text{DFT}_{16}$ (c). The correlation between the two signals is shown in the insert. Comparison between experimental and target operators for $\mathbf{G} = \text{Ha}_{16}$, $F_c = 0.785$ (b) and $\mathbf{G} = \text{DFT}_{16}$, $F_c = 0.818$ (d). The results are obtained without averaging.

$$\text{DFT}_n = \frac{1}{\sqrt{n}} [\omega_n^{jk}]_{j,k=0\dots n-1} \quad \text{with} \quad \omega_n = e^{-2\pi i/n}, \quad (7)$$

and

$$\text{Ha}_n = \frac{1}{\sqrt{n}} \begin{bmatrix} \text{Ha}_{n-1} & \text{Ha}_{n-1} \\ \text{Ha}_{n-1} & -\text{Ha}_{n-1} \end{bmatrix} \quad \text{with} \quad \text{Ha}_1 = [1] \quad (8)$$

with n the size of the operator. We quantify the quality of the operation by estimating the operator's fidelity $F_c = \text{Tr}(|\tilde{\mathbf{G}} \cdot \mathbf{G}^\dagger|^2) * n$ [8], with $\tilde{\mathbf{G}}$ the response matrix of our physical system after projection and \mathbf{G} the target matrix (DFT_n or Ha_n). To characterize the implemented operator $\tilde{\mathbf{G}}$, we sequentially send vectors from an input basis and measure the corresponding outputs fields.

To measure the complex output field, we carry out off-axis holography measurements [48]. It uses a reference arm originating from a 90/10 fiber splitter at the output of the laser. The reference beam and the output of the MMF are recombined using a polarizing beam splitter and a polarizer. The recorded images are post-processed to retrieve the phase information from the interference pattern. Note that the reference arm was not part of the procedure of implementing the linear operator; it is solely used to monitor the effective complex-valued operator $\tilde{\mathbf{G}}$ afterward. (Supplement 1 provides details about the complex field measurements.) Moreover, as a single image allows measuring the complex value output of the operator, interferometric stability over times longer than the integration time of the camera is not required.

We experimentally perform all optical operations according to the presented principle. A large range of input signals is prepared and sent to the setup (see Supplement 1). The quality of our results is assessed by the Pearson correlation coefficient between the absolute values of the experimental and the ideal output vectors \mathbf{C} and also by the experimental fidelity F_c .

In Figs. 3(a) and 3(c), we compare the measured amplitude values obtained for two random input vectors with the expected ones for both operators. The results show good agreement, as emphasized by the correlation coefficients exhibiting values over 95% for these realizations. In Figs. 3(b) and 3(d), we show the real and imaginary parts of the estimated experimental operators $\tilde{\mathbf{G}}$ after normalization and the real and imaginary parts of the target operator \mathbf{G} . The results presented were obtained without averaging. A summary of the measured quality estimators for the MMF experiment is presented in Table 1 with and without averaging for operator sizes of $n = m = 8$ and $n = m = 16$.

A good agreement between the experimental data and the ideal operations outputs is observed for the different sizes tested, even without averaging. It demonstrates the possibility of performing *one shot* operations through a multimode fiber. To further illustrate the possibility to create any desired operator, in Fig. S5 (Supplement 1) we show an experimental implementation of a matrix with no physical meaning displaying the name of the

Table 1. Summary of the Efficiency Results for the MMF Experiment^a

Size	Averaging	C	F_c
$n = m = 8$	1	0.977 ± 0.009	0.973 ± 0.014
$n = m = 8$	10	>0.99	0.996
$n = m = 16$	1	0.912 ± 0.027	0.792 ± 0.027
$n = m = 16$	10	>0.99	0.968

^aC stands for correlation between results and predicted values, and F_c stands for the experimental fidelity.

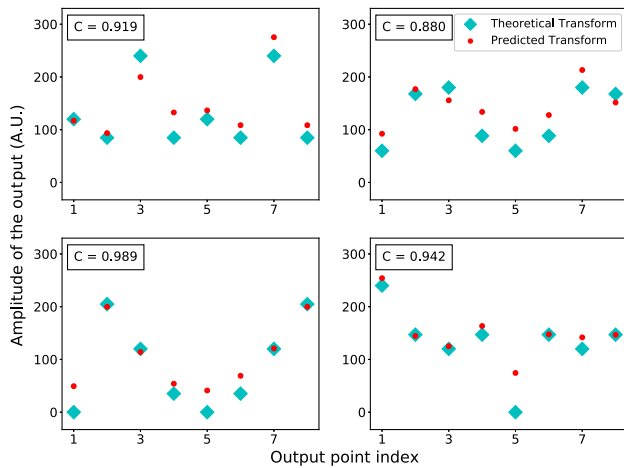


Fig. 4. Amplitude of four different random output vectors for operator $\mathbf{G} = \text{DFT}_8$ obtained using a ground glass diffuser as a complex medium. Cyan diamonds correspond to the theoretical outputs and red dots to the experimental data. Inserts in the top left corners give the correlation between the experimental and the predicted transforms.

authors' host institution by encoding information independently in the real and imaginary part of its elements.

Because the ground glass diffuser experiment is more prone to errors in the operator reconstruction, we only present results for $n = m = 8$. In Fig. 4 we show the raw amplitude of four different outputs for the DFT_8 operator. We measure $\mathbf{C} = 0.948 \pm 0.018$. We estimate that the sources of the errors are the lower laser stability and the nonlinear response of the CCD camera. While negatively affecting the results, we obtain qualitatively similar results, demonstrating the capacity of the approach to work with relatively cheap devices, namely a HeNe laser and a standard CCD camera. Results further illustrating the versatility of our method are displayed in Supplement 1.

5. DISCUSSION

We demonstrated the possibility of using cheap and common media as optical processing units to perform linear operations using wavefront shaping. The attractiveness of such an approach is linked to its ability to be scaled up for larger operations. While we report the implementations of 16×16 operators, much larger operations can be performed, provided there is an increased control over the input field and a reduced noise level. Noticeably, Eq. (2) was only satisfied approximately because of the binary nature of the DMD modulation; the search for such approximation requires computation efforts. While averaging over realizations mitigates the error, a single shot operation is usually desirable. For an ideal amplitude and phase modulation, Eq. (2) can be satisfied exactly with a simple matrix pseudo-inversion. A complete independent amplitude and phase modulation can for example be obtained using two liquid crystal SLMs. Another approach is, after characterization of the medium, to print phase plates to fix the input mask. While limiting the reconfigurability of the system, it reduces the final cost of the processing unit.

For a square target matrix \mathbf{G} , the largest size for which one can find a solution for a fixed number M of controlled modes is $n = m = \sqrt{M}$. Using a multimode fiber as a complex medium, the limiting factor is the number of modes supported by the fiber; for a typical large core step index fiber (550 μm core,

$\text{NA} = 0.22$), $M \approx 60,000$, corresponding to maximal operator dimensions $n = m \approx 250$. In contrast, in scattering layers such as glass diffusers, the number of degrees of freedom available given by the number of propagating modes is quasi unlimited. Thus, the number of independently controlled modes is limited by the number of pixels on the modulator, typically on the order of one million. Note that this remains true in the multiple scattering regime as long as the number of transmission channels is large compared to the number of input pixels (i.e., far away from the localization regime). Hence, this would allow creating linear operators of size $n = m \approx 1000$. These operator sizes match the order of magnitude of the size needed for optical neural networks.

It is important to note that our approach, due to intrinsic losses and the absence of gain in the system, can perform any linear operation only up to a constant multiplier. In particular, it cannot perform operations with above unity singular values. Such a restriction can be detrimental to quantum optics applications where losses can modify the optical state of light. Our apparatus based on DMDs causes more than 50% of the light to be lost upon modulation. However, using a phase-only SLM based on deformable mirrors or a phase plate together with a careful injection into a multimode fiber, close to unitary operations can be achieved. Multimode fibers have the potential to outperform integrated-photonics-based platforms in terms of losses, with insertion losses on the order of 0.3 dB and propagation losses below 1 dB/km, compared to values above 1 dB and 0.1 dB/cm, respectively, for photonic integrated circuits [49].

The presented method requires computational efforts during its calibration; however, once the TM is retrieved and the projectors are calculated, the operations are performed in a single shot ($O(1)$ operations) on a passive system. No further calibration is needed as long as the system is stable. Multimode fibers up to 100 m are stable enough to be used as accurate optical instruments [50]. Stability over multiple days can be obtained by ensuring a controlled environment and good laser stability. Thin diffusers are only limited by the pointing stability. The proposal offers the possibility to implement large optical linear transformations without elaborate fabrication techniques as well as to reconfigure the desired operator without further measurements. Moreover, it opens the opportunity to drastically reduce the energy consumption compared to classical electronic components while increasing the computation speed [11,39]. These characteristics may enable the presented technique to play a key role in the advent of optical analog computation and machine learning.

Funding. Agence Nationale de la Recherche (ANR) (ANR-16-CE25-0008-01 MOLOTOF); Labex WIFI (ANR-10-LABX-24, ANR-10-IDEX-0001-02 PSL*); Ministère de la Défense, Direction Générale de l'Armement (DGA).

Acknowledgment. We thank Yaron Bromberg and Arthur Goetschy for fruitful discussions. We acknowledge Christopher Metzler and Laurent Daudet for sharing phase retrieval codes and providing helpful advice. The datasets generated during the current study are available from the corresponding author upon reasonable request. Interface codes for controlling the DMD are made available at [51], and detailed tutorials to set up DMD experiments are available at [52].

See Supplement 1 for supporting content.

REFERENCES

- P. I. Borel, B. Bilenberg, L. H. Frandsen, T. Nielsen, J. Fage-Pedersen, A. V. Lavrinenko, J. S. Jensen, O. Sigmund, and A. Kristensen, "Imprinted silicon-based nanophotonics," *Opt. Express* **15**, 1261–1266 (2007).
- J. S. Jensen and O. Sigmund, "Topology optimization for nanophotonics," *Laser Photon. Rev.* **5**, 308–321 (2011).
- A. Silva, F. Monticone, G. Castaldi, V. Galdi, A. Alu, and N. Engheta, "Performing mathematical operations with metamaterials," *Science* **343**, 160–163 (2014).
- B. Shen, P. Wang, R. Polson, and R. Menon, "An integrated-nanophotonics polarization beamsplitter with $2.4 \times 2.4 \mu\text{m}^2$ footprint," *Nat. Photonics* **9**, 378–382 (2015).
- A. Y. Piggott, J. Petykiewicz, L. Su, and J. Vučković, "Fabrication-constrained nanophotonic inverse design," *Sci. Rep.* **7**, 1786 (2017).
- M. Reck, A. Zeilinger, H. J. Bernstein, and P. Bertani, "Experimental realization of any discrete unitary operator," *Phys. Rev. Lett.* **73**, 58–61 (1994).
- D. A. B. Miller, "Self-configuring universal linear optical component invited," *Photon. Res.* **1**, 1–15 (2013).
- J. Carolan, C. Harrold, C. Sparrow, E. Martin-Lopez, N. J. Russell, J. W. Silverstone, P. J. Shadbolt, N. Matsuda, M. Oguma, M. Itoh, G. D. Marshall, M. G. Thompson, J. C. F. Matthews, T. Hashimoto, J. L. O'Brien, and A. Laing, "Universal linear optics," *Science* **349**, 711–716 (2015).
- A. Ribeiro, A. Ruocco, L. Vanacker, and W. Bogaerts, "Demonstration of a 4×4 -port universal linear circuit," *Optica* **3**, 1348–1357 (2016).
- A. Annoni, E. Guglielmi, M. Carminati, G. Ferrari, M. Sampietro, D. A. B. Miller, A. Melloni, and F. Morichetti, "Unscrambling light—automatically undoing strong mixing between modes," *Light: Sci. Appl.* **6**, e17110 (2017).
- Y. Shen, N. C. Harris, S. Skirlo, M. Prabhu, T. Baehr-Jones, M. Hochberg, X. Sun, S. Zhao, H. Larochelle, D. Englund, and M. Soljačić, "Deep learning with coherent nanophotonic circuits," *Nat. Photonics* **11**, 441–446 (2017).
- P. L. Mennea, W. R. Clements, D. H. Smith, J. C. Gates, B. J. Metcalf, R. H. S. Bannerman, R. Burgwal, J. J. Renema, W. S. Kolthammer, I. A. Walmsley, and P. G. R. Smith, "Modular linear optical circuits," *Optica* **5**, 1087–1090 (2018).
- R. Bruck, K. Vynck, P. Lalanne, B. Mills, D. J. Thomson, G. Z. Mashanovich, G. T. Reed, and O. L. Muskens, "All-optical spatial light modulator for reconfigurable silicon photonic circuits," *Optica* **3**, 396–402 (2016).
- J.-F. Morizur, L. Nicholls, P. Jian, S. Armstrong, N. Treps, B. Hage, M. Hsu, W. Bowen, J. Janousek, and H.-A. Bachor, "Programmable unitary spatial mode manipulation," *J. Opt. Soc. Am. A* **27**, 2524–2531 (2010).
- G. Labroille, B. Denolle, P. Jian, P. Genevieux, N. Treps, and J.-F. Morizur, "Efficient and mode selective spatial mode multiplexer based on multi-plane light conversion," *Opt. Express* **22**, 15599–15607 (2014).
- I. M. Vellekoop and A. P. Mosk, "Focusing coherent light through opaque strongly scattering media," *Opt. Lett.* **32**, 2309–2311 (2007).
- A. P. Mosk, A. Lagendijk, G. Lerosey, and M. Fink, "Controlling waves in space and time for imaging and focusing in complex media," *Nat. Photonics* **6**, 283–292 (2012).
- S. Rotter and S. Gigan, "Light fields in complex media: mesoscopic scattering meets wave control," *Rev. Mod. Phys.* **89**, 015005 (2017).
- J. W. Goodman, *Speckle Phenomena in Optics: Theory and Applications* (Roberts and Company, 2007).
- S. M. Popoff, G. Lerosey, R. Carminati, M. Fink, A. C. Boccara, and S. Gigan, "Measuring the transmission matrix in optics: an approach to the study and control of light propagation in disordered media," *Phys. Rev. Lett.* **104**, 100601 (2010).
- T. Čižmár and K. Dholakia, "Shaping the light transmission through a multimode optical fibre: complex transformation analysis and applications in biophotonics," *Opt. Express* **19**, 18871–18884 (2011).
- M. Kim, W. Choi, Y. Choi, C. Yoon, and W. Choi, "Transmission matrix of a scattering medium and its applications in biophotonics," *Opt. Express* **23**, 12648–12668 (2015).
- V. Doya, O. Legrand, F. Mortessagne, and C. Miniatura, "Speckle statistics in a chaotic multimode fiber," *Phys. Rev. E* **65**, 056223 (2002).
- C. Draeger and M. Fink, "One-channel time reversal of elastic waves in a chaotic 2D-silicon cavity," *Phys. Rev. Lett.* **79**, 407–410 (1997).
- M. Dupré, P. del Hougne, M. Fink, F. Lemoult, and G. Lerosey, "Wave-field shaping in cavities: Waves trapped in a box with controllable boundaries," *Phys. Rev. Lett.* **115**, 017701 (2015).
- S. M. Popoff, G. Lerosey, M. Fink, A. C. Boccara, and S. Gigan, "Image transmission through an opaque material," *Nat. Commun.* **1**, 1–5 (2010).
- J. Aulbach, B. Gjonaj, P. M. Johnson, A. P. Mosk, and A. Lagendijk, "Control of light transmission through opaque scattering media in space and time," *Phys. Rev. Lett.* **106**, 103901 (2011).
- O. Katz, E. Small, Y. Bromberg, and Y. Silberberg, "Focusing and compression of ultrashort pulses through scattering media," *Nat. Photonics* **5**, 372–377 (2011).
- M. Mounaix, D. Andreoli, H. Defienne, G. Volpe, O. Katz, S. Grésillon, and S. Gigan, "Spatiotemporal coherent control of light through a multiple scattering medium with the multispectral transmission matrix," *Phys. Rev. Lett.* **116**, 253901 (2016).
- P. del Hougne, F. Lemoult, M. Fink, and G. Lerosey, "Spatiotemporal wave front shaping in a microwave cavity," *Phys. Rev. Lett.* **117**, 134302 (2016).
- I. M. Vellekoop, A. Lagendijk, and A. P. Mosk, "Exploiting disorder for perfect focusing," *Nat. Photonics* **4**, 320–322 (2010).
- J.-H. Park, C. Park, H. Yu, J. Park, S. Han, J. Shin, S. H. Ko, K. T. Nam, Y.-H. Cho, and Y. Park, "Subwavelength light focusing using random nanoparticles," *Nat. Photonics* **7**, 454–458 (2013).
- A. Liutkus, D. Martina, S. Popoff, G. Chardon, O. Katz, G. Lerosey, S. Gigan, L. Daudet, and I. Carron, "Imaging with nature: compressive imaging using a multiply scattering medium," *Sci. Rep.* **4**, 5552 (2015).
- S. R. Huisman, T. J. Huisman, S. A. Goorden, A. P. Mosk, and P. W. H. Pinkse, "Programming balanced optical beam splitters in white paint," *Opt. Express* **22**, 8320–8332 (2014).
- S. R. Huisman, T. J. Huisman, T. A. W. Wolterink, A. P. Mosk, and P. W. H. Pinkse, "Programmable multipoint optical circuits in opaque scattering materials," *Opt. Express* **23**, 3102–3116 (2015).
- H. Defienne, M. Barbieri, I. A. Walmsley, B. J. Smith, and S. Gigan, "Two-photon quantum walk in a multimode fiber," *Sci. Adv.* **2**, e1501054 (2016).
- T. A. W. Wolterink, R. Uppu, G. Cstis, W. L. Vos, K.-J. Boller, and P. W. H. Pinkse, "Programmable two-photon quantum interference in 103 channels in opaque scattering media," *Phys. Rev. A* **93**, 053817 (2016).
- R. Fickler, M. Ginoya, and R. W. Boyd, "Custom-tailored spatial mode sorting by controlled random scattering," *Phys. Rev. B* **95**, 161108 (2017).
- P. del Hougne and G. Lerosey, "Leveraging chaos for wave-based analog computation: Demonstration with indoor wireless communication signals," *Phys. Rev. X* **8**, 041037 (2018).
- A. Goetschy and A. D. Stone, "Filtering random matrices: the effect of incomplete channel control in multiple scattering," *Phys. Rev. Lett.* **111**, 063901 (2013).
- S. M. Popoff, A. Goetschy, S. F. Liew, A. D. Stone, and H. Cao, "Coherent control of total transmission of light through disordered media," *Phys. Rev. Lett.* **112**, 133903 (2014).
- V. A. Marcenko and L. A. Pastur, "Distribution of eigenvalues for some sets of random matrices," *Mat. Sb.* **1**, 457–483 (1967).
- W. Xiong, P. Ambichl, Y. Bromberg, B. Redding, S. Rotter, and H. Cao, "Principal modes in multimode fibers: exploring the crossover from weak to strong mode coupling," *Opt. Express* **25**, 2709–2724 (2017).
- A. Drémeau, A. Liutkus, D. Martina, O. Katz, C. Schülke, F. Krzakala, S. Gigan, and L. Daudet, "Reference-less measurement of the transmission matrix of a highly scattering material using a DMD and phase retrieval techniques," *Opt. Express* **23**, 11898–11911 (2015).
- C. A. Metzler, M. K. Sharma, S. Nagesh, R. G. Baraniuk, O. Cossairt, and A. Veeraraghavan, "Coherent inverse scattering via transmission matrices: Efficient phase retrieval algorithms and a public dataset," in *IEEE International Conference on Computational Photography (ICCP)* (IEEE, 2017).
- "Gurobi Optimizer Reference Manual, V.8.1" (Gurobi Optimization, 2018). <http://www.gurobi.com/documentation/8.1/refman/refman.html>
- S. Diamond and S. Boyd, "Cvxpy: a python-embedded modeling language for convex optimization," *J. Mach. Learn. Res.* **17**, 1–5 (2016).

48. E. Cuche, P. Marquet, and C. Depeursinge, "Simultaneous amplitude-contrast and quantitative phase-contrast microscopy by numerical reconstruction of Fresnel off-axis holograms," *Appl. Opt.* **38**, 6994–7001 (1999).
49. S. J. McNab, N. Moll, and Y. A. Vlasov, "Ultra-low loss photonic integrated circuit with membrane-type photonic crystal waveguides," *Opt. Express* **11**, 2927–2939 (2003).
50. B. Redding, S. M. Popoff, and H. Cao, "All-fiber spectrometer based on speckle pattern reconstruction," *Opt. Express* **21**, 6584–6600 (2013).
51. S. M. Popoff and M. W. Matthès, "ALP4lib: a Python module to control Vialux DMDs" (Zenodo, 2016). <https://zenodo.org/record/1160714#.XJl2PZnKhUM>
52. "Wavefront shaping techniques in complex media," <http://wavefrontshaping.net>.